Effect of Obstacle Shape on Flame Acceleration and Transition to Detonation in an Obstructed Channel

Xiao H.[1],*, Oran E.S.[2]

[1] *State Key Laboratory of Fire Science, University of Science and Technology of China, Hefei, Anhui Province, China*

[2] *Department of Aerospace Engineering, University of Maryland, College Park, Maryland, USA*

**Corresponding author's email: xiaoh@ustc.edu.cn*

ABSTRACT

Numerical simulations were conducted to understand the effect of obstacle shape on flame acceleration and deflagration-to-detonation transition (DDT) through an array of obstacles in a channel. The multi-dimensional, fully compressible reactive Navier-Stokes equations, coupled to a calibrated chemical-diffusive model for combustion of a stoichiometric hydrogen-air mixture, were solved using a high-order algorithm with adaptive mesh refinement (AMR). While maintaining the same blockage ratio, the influence of obstacle shape on DDT was examined with circular, square, and triangular obstacles. The simulations show that the shape of the obstacle plays an important role in flame acceleration and detonation initiation. Squares create spaces between obstacles and walls, and these spaces provide a path that leads to the fastest flame acceleration and shortest detonation initiation time compared to circular and triangle obstacles. The presence of sharp angles on the triangular obstacles is favorable for flame stretching and convolution, and this facilitates flame acceleration and transition to detonation. The round, circular obstacles have the least effect on promoting flame acceleration and DDT. Although there are differences in flame acceleration and DDT among differently shaped obstacles, the basic mechanism for detonation initiation is similar in all of the cases studied and involves shock interactions with flame front.

KEYWORDS: Flame acceleration, deflagration-to-detonation transition, obstacle shape, numerical simulation.

INTRODUCTION

Flame acceleration and deflagration-to-detonation transition (DDT) is an important topic in the research areas of explosion safety [1-6] and combustion applications [7-9]. The physics in the process is very complex and involves flow instabilities, turbulence, shock-flame and shock-shock interactions, boundary layer, and detonation initiation. Significant progress has been made in modeling and understanding DDT in recent years [2, 4, 10-15]. Nonetheless, many of the fundamental mechanisms of DDT are not fully understood and numerical simulations remain a significant challenge for these very fast, nonlinear, stochastic process.

Obstructed channels are often used to study flame acceleration and DDT in a controlled manner in both experiments and numerical simulations [1, 2, 4, 5, 8, 13, 14, 16]. The basic mechanisms underlying flame acceleration in obstacle-laden channels involve thermal expansion of hot combustion products, flame-vortex interaction, acoustic-shock-flame interactions, Kelvin-Helmholtz (KH), Rayleigh-Taylor (RT), and Richtmyer-Meshkov (RM) instabilities. These phenomena result in a turbulent flame that further accelerates the flow. The accelerating flow produces strong shocks ahead of flame front and creates conditions under which DDT can occur. Detonations can be triggered by Zeldovich's reactivity-gradient mechanism once hot spots are

Proceedings of the Ninth International Seminar on Fire and Explosion Hazards (ISFEH9), pp. 279-288
Edited by Snegirev A., Liu N.A., Tamanini F., Bradley D., Molkov V., and Chaumeix N.
Published by St. Petersburg Polytechnic University Press
ISBN: 978-5-7422-6496-5 DOI: 10.18720/spbpu/2/k19-111

created by boundary layer effects, Mach-stem reflections from obstacles, or turbulent mixing [2, 4, 13-15]. Another possible mechanism of DDT is direct initiation of detonation arising from shock focusing, which occurs when a critical amount of energy is deposited in a very small region of space [10, 11, 17].

The configuration or layout of obstacles plays a role in flame acceleration and DDT in channels [12, 18-21]. Practical applications can involve arrays of obstacles, such as pipelines in chemical processing plant, cooling pipes in power plants, and vessels in fuel storage facilities. Ogawa et al. investigated flame acceleration and DDT through an array of cylindrical [19, 22] or square [12] obstacles in an unconfined region. They found that in the early stages, the flame accelerates more rapidly in the directions without obstruction. As shock waves are generated in the later stages, interactions of shocks with flames dominate the flow-acceleration process, and the flame accelerates faster in more obstructed directions. Detonation initiation eventually occurs through the hot-spot mechanism in the more obstructed directions. Quasi-detonation was observed in the final stage of reaction wave propagation. Specifically, for the cylinder array, DDT could not occur when the obstacles were aligned parallel to the direction of flame propagation. Pinos and Ciccarelli [18] performed experiments of to examine the propagation of flame and detonation in a channel with an array of cylinders. It was found that the initial flame acceleration is significantly influenced by the blockage ratio instead of obstacle layout. The combustion wave also propagates as a quasi-detonation wave in the later stage. The previous studies considered a single obstacle shape, either square or cylindrical. These studies, however, did not consider the effect of obstacle shape.

In this study, we perform numerical simulations of flame acceleration and DDT through an array of obstacles of different shapes in a channel. This is done by solving the unsteady, fully compressible, reactive Navier-Stokes equations with adaptive mesh refinement (AMR).

PHYSICAL MODEL AND NUMERICAL METHOD

The governing equations solved in the numerical simulations are the two-dimensional (2D) fully compressible Navier-Stokes equations and conservation equations of mass, energy and species [2, 23]:

$$\frac{\partial \rho}{\partial t} + \nabla \cdot (\rho \vec{u}) = 0 , \tag{1}$$

$$\frac{\partial (\rho \vec{u})}{\partial t} + \nabla \cdot (\rho \vec{u}\vec{u}) + \nabla p = \nabla \cdot \hat{\tau} , \tag{2}$$

$$\frac{\partial (\rho E)}{\partial t} + \nabla \cdot \left((\rho E + p)\vec{u} \right) = \nabla \cdot (\vec{u} \cdot \hat{\tau}) + \nabla \cdot (K \nabla T) - \rho q \dot{\omega} , \tag{3}$$

$$\frac{\partial (\rho Y)}{\partial t} + \nabla \cdot (\rho Y \vec{u}) + \nabla \cdot (\rho D \nabla Y) = \rho \dot{\omega} , \tag{4}$$

$$p = \rho RT / M , \tag{5}$$

$$\hat{\tau} = \rho \nu ((\nabla \vec{u}) - (\nabla \vec{u})^{Tr} - \frac{2}{3} (\nabla \cdot \vec{u}) I) , \tag{6}$$

$$E = \frac{p}{(\gamma - 1)\rho} + \frac{1}{2} (\vec{u} \cdot \vec{u}) , \tag{7}$$

where t is the time, ρ is the density, p is the pressure, $\vec{u}$ is the vector velocity, E is the specific total energy, T is the temperature, q is the chemical energy release, Y is the mass fraction, $\dot{\omega}$ is the chemical reaction rate, D is the mass diffusivity, K is the thermal conductivity, R is the universal gas constant, M is the molecular weight, $\hat{\tau}$ is the viscous stress tensor, ν is the kinematic viscosity, I is the unit tensor, and γ is the specific heat ratio. The superscript Tr denotes matrix transportation.

The combustion of premixed stoichiometric hydrogen and air is modeled by a chemical-diffusive model (CDM) [24], for which the reaction rate is defined as:

$$\dot{\omega} = \frac{dY}{dt} = -A\rho Y \exp\left(-\frac{E_a}{RT}\right), \tag{8}$$

where A and E_a are the pre-exponential factor and activation energy, respectively.

The diffusion properties of the gas mixture are calculated as a function of temperature:

$$\mu = \mu_0 T^{0.7}, \; D = D_0 T^{0.7}, \; k = k_0 T^{0.7}, \tag{9}$$

where μ and k are the dynamic viscosity and thermal diffusivity, respectively. Parameters μ_0, D_0, and k_0 are the reference coefficients. The input parameters of the CDM are given in [13]. The CDM reproduces the major properties of laminar and turbulent flames, detonation, and the transitions among these states. The model has been tested extensively and used to solve a variety of combustion problems, including laminar flame [23, 25, 26] and turbulent flame [27, 28] dynamics, cellular detonation structure [29, 30], and DDT [1, 2, 4, 10, 11, 13, 14].

The governing equations are solved by using a third-order WENO algorithm with HLLC Riemann solver. Time integration is advanced using a second-order Runge-Kutta algorithm. The computational grid is generated by dynamically adaptive mesh refinement (AMR) [31]. AMR allows the computations to resolve important features of flow, such as flame, strong pressure waves, and boundary layers.

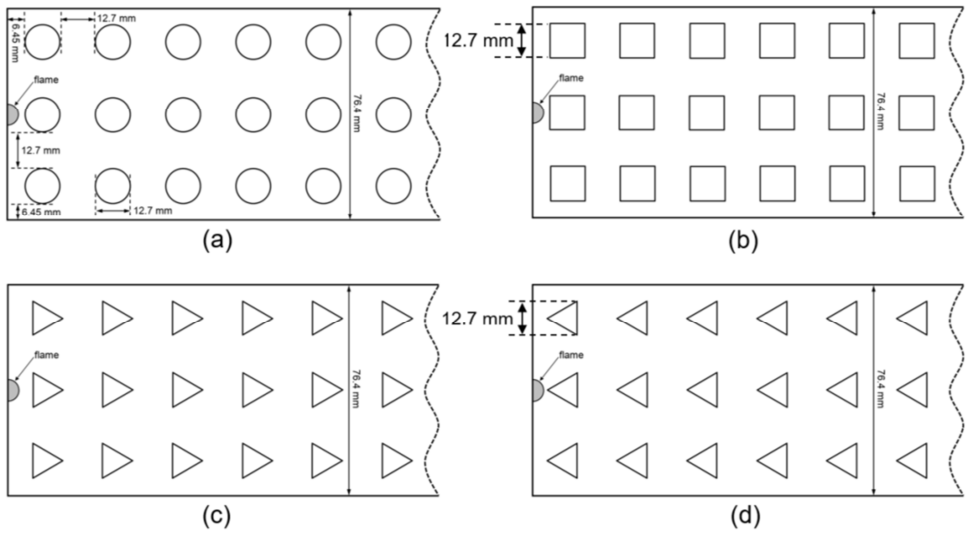

Fig. 1. Computational domain with an array of obstacles of different shapes. (a) Circular obstacles [25]; (b) Square obstacles; (c) Right triangular obstacles; (d) Left triangular obstacles. No-slip, adiabatic, and reflecting boundaries are used for the channel walls and obstacle surfaces. The radius of the initial flame (a semi-circular ignition zone) is 1 mm.

The computational domain with an array of obstacles of different shapes is shown schematically in Fig. 1. The dommain is a 76.4 mm high channel with an array of obstacles that are aligned parallel to the direction of flame propagation. Fig. 1a shows parallel rows of cylindrical obstacles with a blockage ratio 0.5. The radius of the cylinders is 12.7 mm. This setup was used to simulate the experiment in [18] and showed reasonable agreement with the experimental observations [25]. Three additional obstacle shapes were considered in the calculations, i.e., squares (Fig. 1b), right isosceles triangles (Fig. 1c), and left isosceles triangles (Fig. 1d). The edge of the squares and sides of the triangles are 12.7 mm. The blockage ratio of the channel and the geometrical center of the obstacles are the same as that for the case with cylindrical obstacles.

No-slip, reflecting, and adiabatic boundary conditions were used at all the walls of the channel and obstacle surfaces. The flame was ignited by placing a semi-circular region of hot, burned gas with a radius of 1 mm at the left wall at t = 0. Grid resolution tests were performed using three different minimum grid sizes, dx_{min} = 1/67, 1/134 and 1/268 cm. A minimum size of dx_{min} = 1/268 (37.3 μm), corresponding to 10 cells in the flame and 5 cells in half-reaction thickness at initial conditions, was sufficient to capture the major features of flame acceleration and DDT.

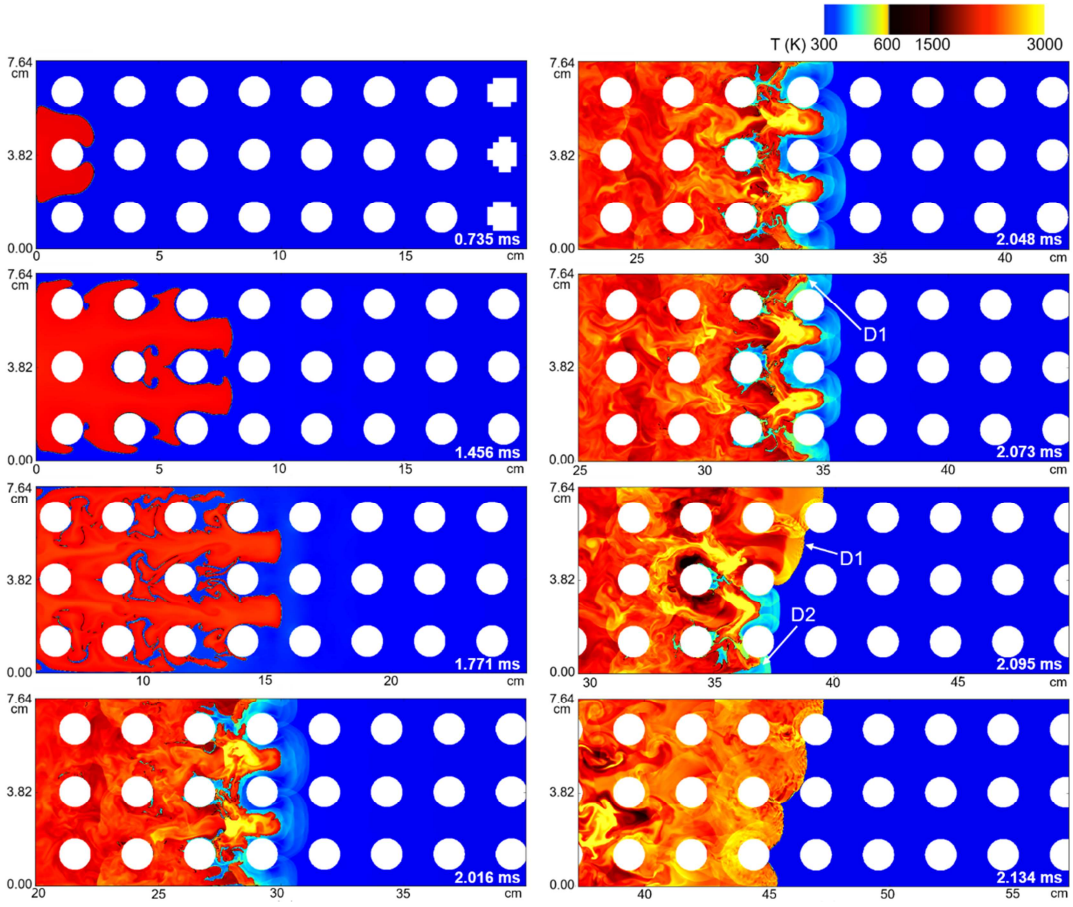

Fig. 2. Temperature fields of flame acceleration and DDT in a channel with an array of cylindrical obstacles. D1: first detonation; D2: second detonation.

RESULTS AND DISCUSSION

Flame accleration and DDT process

A sequence of temperature fields is shown in Fig. 2. From these, we note the flame acceleration and see when and where DDT occurred. The early flame acceleration results primarily from thermal expansion of the combustion products. In the unobstructed directions, the flame is elongated as it passes over the obstacles, as shown at 0.735 ms. The flame is convoluted as it stretches in obstacle wakes (see 1.456 and 1.771 ms). Flame-vortex interactions cause more growth in flame surface area, as shown at 1.771 ms. These effects lead to considerable increase in flame surface area and, consequently, to flame acceleration. As the flame continues to accelerate, strong pressure waves and shock waves are generated, as shown at 2.016 ms. This results in significant compression of unburned gas and more flame instabilities, such as Rayleigh-Taylor and Richtmyer-Meshkov instabilities. These effects cause further flame acceleration and thus produce a strong leading shock wave downstream of the flame front (see 2.048 and 2.073 ms). A detonation, D1, is triggered near the upper wall due to shock focusing [25], and it proceeds to sweep through unburned gas. Before the detonation reaches to the obstacles next to the lower wall, however, a second detonation, D2, arises near the lower wall. These two detonations soon unite to one, which travels into the remainder of the unburned gas. In the cases with the other obstacles shapes, detonation initiation occurs in a similar way, although there are differences in flame acceleration due to different obstacle shapes.

Effect of obstacle shape on flame acceleration and DDT

Figure 3 shows the location of leading edge of the reaction front as a function of time for different obstacle shapes. The sudden inflection of each curve corresponds to DDT. It shows that flame acceleration and detonation initiation are different with different obstacle shapes. The time to detonation initiation varies from 1.626 ms for the square to 2.072 ms for the circle. The flame accelerates significantly faster and the detonation occurs at a shorter time with square obstacles. The overall flame propagation and DDT with right and left triangles are essentially the same, with only small differences between left-facing and right-facing triangles. This means the specific arrangement or directions of the triangle obstacles considered in the calculations has only a limited influence on the flame acceleration and DDT.

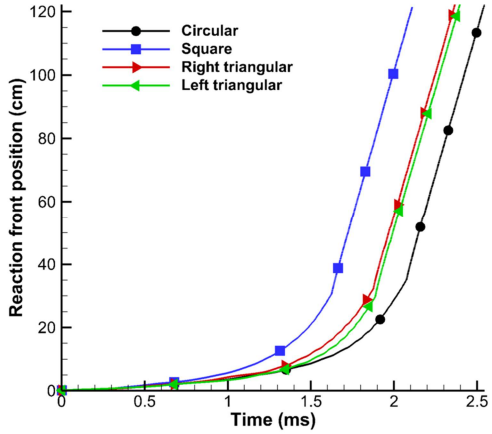

Fig. 3. Position of leading edge of reaction front as a function of time for different types of obstacle.

Table 1 shows the obstacle area for each type of obstacle, as normalized by the area of circle obstacle. Combining the information from Table 1 with the flame-acceleration curves in Fig. 3, we see that flame acceleration does not necessarily correlate with the obstacle area. Although the square

shape with the largest area produces the fastest flame, the triangle shape with the smallest area leads to more rapid flame acceleration and and earlier DDT occurrence than the cylindrical shape.

Table 1. Normalized area of obstacle with different shapes

	Circle	Square	Right triangle	Left triangle
Normalized obstacle area	1	1.27	0.55	0.55

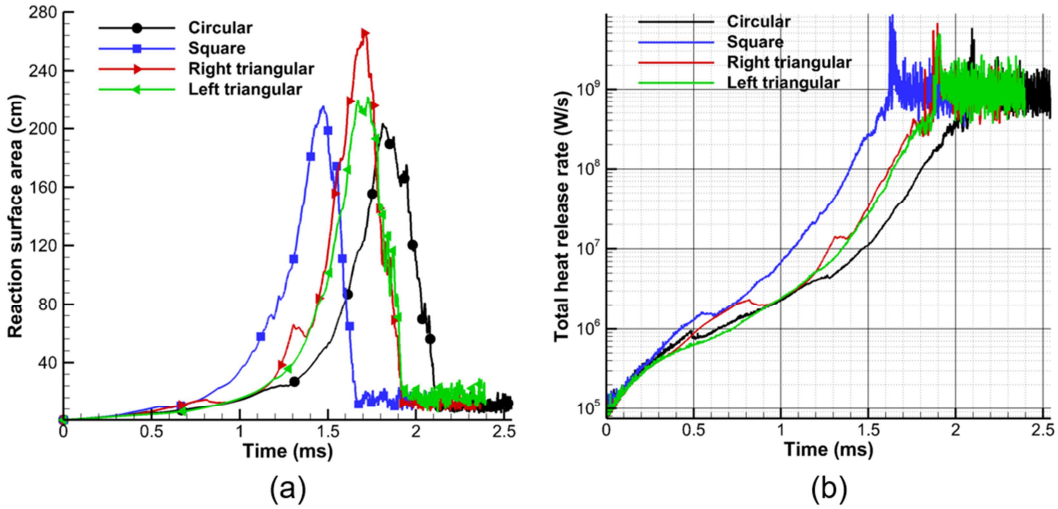

Fig. 4. Surface area of reaction front (a) and total heat release rate (b) as a function of time for different obstacle shapes.

Figure 4 shows (a) the surface area of reaction front and (b) the total heat-release rate, both as a function of time for different obstacle shapes. From early in the calculation, the square obstacle creates a larger flame surface area (Fig. 4a), and so it shows a higher total heat-release rate (Fig. 4b). The reason for this is that the spaces between the obstacles and between obstacles and walls serve as narrow channels that can lead to rapid increase in flame surface area and large flame acceleration [32, 33], as shown in Fig. 5.

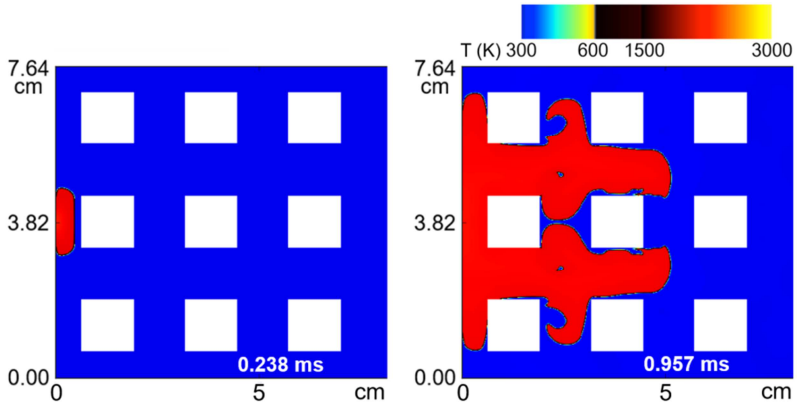

Fig. 5. Selected temperature maps showing flames at early stage with square obstacles.

Figure 6 shows selected temperature fields of flames propagating through right-facing (a) and left-facing triangular obstacles. As shown in Fig. 3, the presence of sharp angles in the triangles causes more flame stretching or convolution than that produced by circular obstacles, which results in quicker growth of flame surface area and thus higher flame acceleration. In the case with right-facing triangles, the flame develops more small structures in the early stages than it does with left-facing triangles, as shown at 0.601 and 1.299 ms in Fig. 6a. Nonetheless, the flame with left-facing triangles tends to expand more in the transverse direction (see flames at 1.299 and 1.702 ms in Fig. 6b), which compensates for the difference in flame surface area. These effects show why the differences in flame acceleration and DDT between right- and left-facing triangles are quite minor (see Figs. 4 and 5).

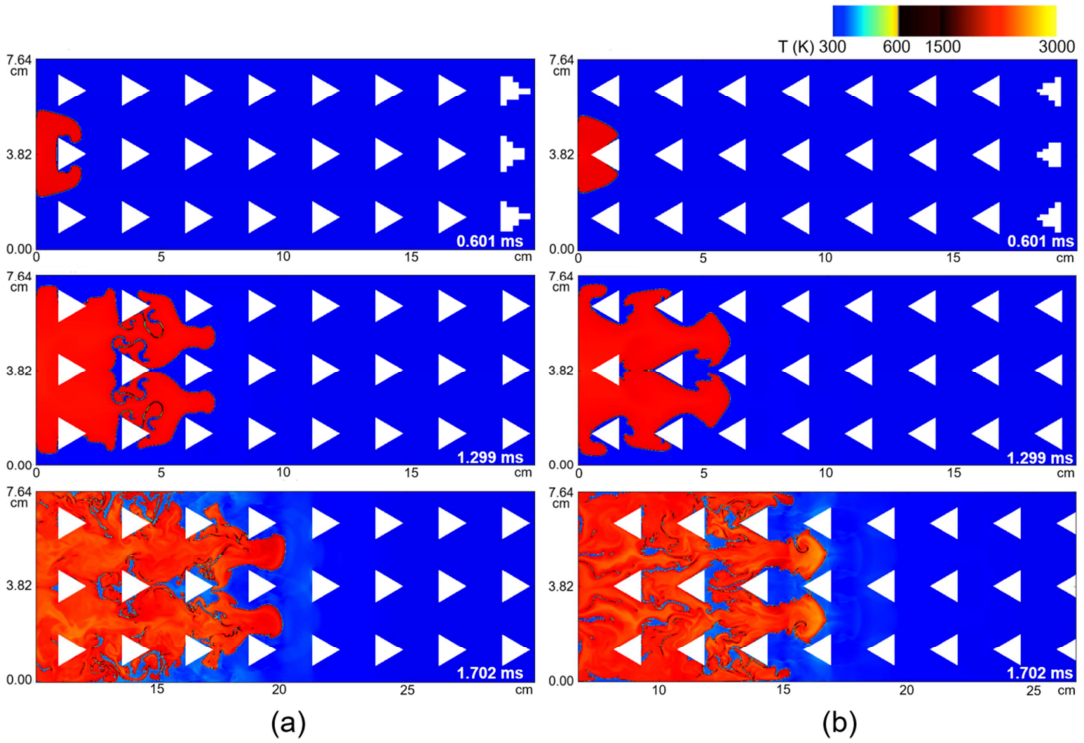

Fig. 6. Temperature fields of flame acceleration through an array of (a) right triangles and (b) left triangles.

Figure 7 shows the propagation speed of the leading edge of the reaction front as a function of distance traveled for different obstacle shapes. Overall, the flame acceleration and DDT are similar for all of the obstacle shapes. In the flame acceleration stage, the speed of the flame front oscillates when the flame passes over every row of obstacles. The amplitude of the oscillation increases with increasing the speed. There is a short time when the flame is in the choking regime, in which the flame generally travels at an average speed that is typically from 1/3 to 1/2 of (Chapman-Jouguet) CJ detonation velocity. Here the average speed of flame front is almost constant, about 800 m/s. In the meantime, the oscillation amplitude also decreases noticeably in the choking regime. The position of detonation initiation for all cases is from 30 cm for left-facing triangles to 35 cm for the circular obstacles. The trend for the location of detonation initiation is different from that of the time for detonation initiation (see Fig. 3). The square obstacles have the shortest time to detonation initiation, but the location of detonation is further downstream than that of the left-facing triangles. Nonetheless, the difference in detonation initiation location between square and triangle obstacles is very small. It is known that detonation initiation is a stochastic phenomenon in nature [2, 4].

Practically, this means small variations in the background conditions *may* trigger considerable differences in detonation initiation location. In the present simulations, the difference in obstacle shape may lead to the stochasticity in the detonation initiation.

For all cases studied, the speed of the reaction front oscillates over a wide range after detonation initiation because of the repeated detonation failures and reignitions. When a detonation failure occurs, the detonation decouples into a flame and shock wave, which cause a sudden decrease in speed of reaction front. When a detonation is reignited, a overdriven detonation is formed with a speed higher than CJ detonation velocity.

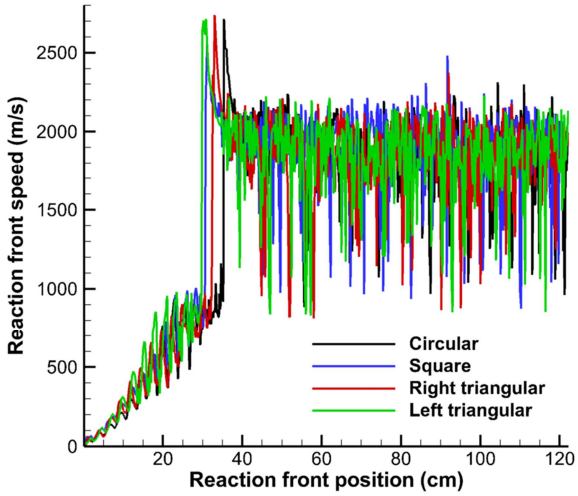

Fig. 7. Speed of leading edge of reaction front as a function of position for obstacles of different shapes.

CONCLUSIONS

A series of numerical simulations was performed to study flame acceleration and DDT through arrays of obstacles in a channel filled with stoichiometric hydrogen-air mixture. A third-order WENO method with AMR was used in the computations to solve the unsteady, multidimensional, fully compressible Navier-Stokes equations coupled with a simplified calibrated chemical-diffusive model (CDM). The thermochemical parameters of the CDM were chosen to represent the combustion of the hydrogen-air mixture. Four different obstacle shapes, with the same blockage ratio of 0.5, were studied to show the effect of obstacle shape on flame acceleration and transition to detonation.

The simulations show that flame acceleration is greatly influenced by the flame-vortex interaction and flame stretching, which causes the flame surface area to increase as it passes over obstacles. The flame speed begins to decrease each time the flame propagates over a row of obstacles, and this decrease results in oscillations in flame speed. In the later stages of flame acceleration, flame-shock and shock-shock interactions dominate the flame acceleration. Detonation was initiated by shock interactions downstream of the flame front or at flame front. After detonation initiation, the reaction front propagated as a quasi-detonation with frequent detonation failure and reignition. The obstacle shape had a significant effect on the flame acceleration and detonation initiation, although the basic mechanism of DDT was similar for all of the shapes simulated.

For square obstacles, the obstacle-obstacle and obstacle-wall spaces acted as narrow channels and led to faster flame acceleration and a shorter time to detonation than the circular and triangular obstacles. For triangular obstacles, the sharp angles of the obstacles is conducive to flame stretching

or convolution that promotes flame acceleration and transition to detonation. Nonetheless, the specific direction of the obstacle layout (left- or right-facing triangles) considered in this work has only a small effect on the flame acceleration and DDT. The circular obstacles have the least effect on enhancing flame acceleration and DDT, since the round shape is less favorable for flame stretching or convolution. In addition, the results show that the effect of obstacle shape does not correlate with obstacle area.

ACKNOWLEDGMENTS

This study was supported by University of Science and Technology of China through the "100 Talents Project" of Chinese Academy of Sciences and the Alpha Foundation (Grant No. AFC215FO-73). The views, opinions and recommendations expressed herein are solely those of the authors and do not imply any endorsement by the Alpha Foundation, its Directors and staff. The authors are also thankful for the support provided by the University of Maryland through Minta Martin Endowment Funds in the Department of Aerospace Engineering, the A. James Clark Distinguished Chair and the Glenn L. Martin Institute Chaired Professorship at the A. James Clark School of Engineering. The authors acknowledge the University of Maryland super-computing resources (http://www.it.umd.edu/hpcc) made available in performing the research reported in this paper.

REFERENCES

[1] E.S. Oran, From catastrophic accidents to the creation fo the universe, Proc. Combust. Inst. 35 (2015) 1-35.

[2] D.A. Kessler, V.N. Gamezo, E.S. Oran, Simulations of flame acceleration and deflagration-to-detonation transitions in methane-air systems, Combust. Flame 157 (2010) 2063-2077.

[3] P. Middha, O.R. Hansen, Predicting deflagration to detonation transition in hydrogen explosions, Process Saf. Progr. 27 (2008) 192-204.

[4] E.S. Oran, V.N. Gamezo, Origins of the deflagration-to-detonation transition in gas-phase combustion, Combust. Flame 148 (2007) 4-47.

[5] G. Ciccarelli, S. Dorofeev, Flame acceleration and transition to detonation in ducts, Progr. Energy Combust. Sci. 34 (2008) 499-550.

[6] M. Kuznetsov, G. Ciccarelli, S. Dorofeev, V. Alekseev, Y. Yankin, T.H. Kim, DDT in methane-air mixtures, Shock Waves 12 (2002) 215-220.

[7] Y. Huang, H. Tang, J. Li, J. Wang, Deflagration-to-detonation transition of kerosene-air mixtures in a small-scale pulse detonation engine, Proceedings of the Institution of Mechanical Engineers Part G-J. Aerosp. Eng. 225 (2011) 441-448.

[8] G.D. Roy, S.M. Frolov, A.A. Borisov, D.W. Netzer, Pulse detonation propulsion: challenges, current status, and future perspective, Progr. Energy Combust. Sci. 30 (2004) 545-672.

[9] P. Wolanski, Detonative propulsion, Proc. Combust. Inst. 34 (2013) 125-158.

[10] G.B. Goodwin, R.W. Houim, E.S. Oran, Shock transition to detonation in channels with obstacles, Proc. Combust. Inst. 36 (2017) 2717-2724.

[11] G.B. Goodwin, R.W. Houim, E.S. Oran, Effect of decreasing blockage ratio on DDT in small channels with obstacles, Combust. Flame 173 (2016) 16-26.

[12] T. Ogawa, V.N. Gamezo, E.S. Oran, Flame acceleration and transition to detonation in an array of square obstacles, J. Loss Prev. Process Ind. 26 (2013) 355-362.

[13] V.N. Gamezo, T. Ogawa, E.S. Oran, Flame acceleration and DDT in channels with obstacles: Effect of obstacle spacing, Combust. Flame 155 (2008) 302-315.

[14] V.N. Gamezo, T. Ogawa, E.S. Oran, Numerical simulations of flame propagation and DDT in obstructed channels filled with hydrogen-air mixture, Proc. Combust. Inst. 31 (2007) 2463-2471.

[15] R.W. Houim, A. Ozgen, E.S. Oran, The role of spontaneous waves in the deflagration-to-detonation transition in submillimetre channels, Combust. Theory Model. 20 (2016) 1068-1087.

[16] T. Obara, T. Kobayashi, S. Ohyagi, Mechanism of deflagration-to-detonation transitions above repeated obstacles, Shock Waves 22 (2012) 627-639.

[17] S. Maeda, S. Minami, D. Okamoto, T. Obara, Visualization of deflagration-to-detonation transitions in a channel with repeated obstacles using a hydrogen-oxygen mixture, Shock Waves 26 (2016) 573-586.

[18] T. Pinos, G. Ciccarelli, Combustion wave propagation through a bank of cross-flow cylinders, Combust. Flame 162 (2015) 3254-3262.

[19] T. Ogawa, E.S. Oran, V.N. Gamezo, Numerical study on flame acceleration and DDT in an inclined array of cylinders using an AMR technique, Comput. Fluids 85 (2013) 63-70.

[20] G. Ciccarelli, C. Johansen, M. Parravani, Transition in the propagation mechanism during flame acceleration in porous media, Proc. Combust. Inst. 33 (2011) 2273-2278.

[21] J. Chao, J.H.S. Lee, The propagation mechanism of high speed turbulent deflagrations, Shock Waves 12 (2003) 277-289.

[22] T. Ogawa, V.N. Gamezo, E.S. Oran, Flame acceleration and transition to detonation in an array of cylinders, In: 23rd International Colloquium on the Dynamics of Explosions and Reactive Systems, Irvine, USA, 2011.

[23] H. Xiao, R.W. Houim, E.S. Oran, Formation and evolution of distorted tulip flames, Combust. Flame 162 (2015) 4084–4101.

[24] C.R. Kaplan, A. Ozgen, E.S. Oran, Chemical-diffusive models for flame acceleration and transition-to-detonation: genetic algorithm and optimisation procedure, Combust. Theor. Model. 23 (2019) 67-86.

[25] H. Xiao, R.W. Houim, E.S. Oran, Flame acceleration and defagration-to-detonation transition through an array of obstacles, In: 26th International Colloquium on the Dynamics of Explosions and Reactive Systems, Boston, MA, USA, 2017.

[26] V.N. Gamezo, E.S. Oran, Flame acceleration in narrow channels: applications for micropropulsion in low-gravity environments, AIAA J. 44 (2006) 329-336.

[27] A.Y. Poludnenko, E.S. Oran, The interaction of high-speed turbulence with flames: Turbulent flame speed, Combust. Flame 158 (2011) 301-326.

[28] A.Y. Poludnenko, E.S. Oran, The interaction of high-speed turbulence with flames: Global properties and internal flame structure, Combust. Flame 157 (2010) 995-1011.

[29] V.N. Gamezo, A.A. Vasil'ev, A.M. Khokhlov, E.S. Oran, Fine cellular structures produced by marginal detonations, Proc. Combust. Inst. 28 (2000) 611-617.

[30] D.A. Kessler, V.N. Gamezo, E.S. Oran, Multilevel detonation cell structures in methane-air mixtures, Proc. Combust. Inst. 33 (2011) 2211-2218.

[31] Boxlib, Center for Computational Sciences and Engineering, University of California, Berkeley. https://ccse.lbl.gov/BoxLib/index.html Data Retrieved in December 2015).

[32] V. Bychkov, V. Akkerman, G. Fru, A. Petchenko, L.E. Eriksson, Flame acceleration in the early stages of burning in tubes, Combust. Flame 150 (2007) 263-276.

[33] C. Clanet, G. Searby, On the "tulip flame" phenomenon, Combust. Flame 105 (1996) 225-238.